HiSST: 3rd International Conference on
High-Speed Vehicle Science Technology
14 -19 April 2024, Busan, Korea

# Internal flow path analysis of the Scramjet Hypersonic Experimental Vehicle

*O. Russo[1], P. Roncioni[2], M. Marini[3], S. Di Benedetto[4], G. Ranuzzi[5], S. Pizzurro[6]*

## Abstract

The paper focuses on the assessment of propulsive and combustion performances of a scramjet engine in hypersonic cruise conditions and its emission indexes for various species involved in the non-premixed combustion process. Nose-to-tail CFD analysis of the entire internal flow path (inlet, combustor and nozzle) are performed in flight-cruise configuration, for both fuel-off and fuel-on conditions, by using ANSYS FLUENT software with steady RANS modelling with available literature chemical schemes. The performance parameters, such as combustion efficiency and kinetic and thermodynamic quantities, revealed a significant improvement as well as the achievement of very high combustion efficiency by the end of the engine cycle is achieved.

**Keywords:** *Scramjet, hypersonic, CFD, supersonic combustion, emission indexes*

**Nomenclature:**

ASI – Italian Space Agency
CFD – Computational Fluid Dynamics
CIRA – Italian Aerospace Research Centre
ER – Equivalence Ratio
MFR – Mass Flow Rate
SCRAMJET – Supersonic Combustion Ramjet
SHEV – Scramjet Hypersonic Experimental Vehicle
$\eta_c$ – combustion efficiency

## 1. Introduction

In the *SCRAMJET* engine, combustion takes place at supersonic speed and allows its use for vehicles operating in a flight regime with a Mach number higher than 5, called hypersonic regime. The aircrafts operating in this regime are also called *hypersonic vehicles*. Unlike conventional jet engines, air compression in scramjet engines occurs due to its simple geometry as it has no rotating parts like the turbine, which is a problem when the temperature in the combustion chamber becomes high and this limits operation of the engine to a low Mach number.
In the frame of the national program of aerospace research, PRO.R.A., CIRA, taking advantage from to its strong involvement in the European projects and in particular in HEXAFLY-INTernational (flight test of an unpropelled vehicle for hypersonic flight) and previously in HEXAFLY, posed the challenge of designing a scramjet hypersonic demonstrator for a future test in-flight, named *Scramjet Hypersonic Experimental Vehicle*, i.e., SHEV. In 2022, as the project was of high interest also of the Italian Space Agency (ASI), the two national entities decided to co-fund the research activities by a dedicated

[1] *Italian Aerospace Research Centre (CIRA), Via Maiorise snc, 81043 Capua, Italy, Email: o.russo@cira.it*
[2] *Italian Aerospace Research Centre (CIRA), Via Maiorise snc, 81043 Capua, Italy, Email: p.roncioni@cira.it*
[3] *Italian Aerospace Research Centre (CIRA), Via Maiorise snc, 81043 Capua, Italy, Email: m.marini@cira.it*
[4] *Italian Aerospace Research Centre (CIRA), Via Maiorise snc, 81043 Capua, Italy, Email: s.dibenedetto@cira.it*
[5] *Italian Space Agency (ASI), Via del Politecnico snc, 00133 Rome, Italy, Email: giuliano.ranuzzi@asi.it*
[6] *Italian Space Agency (ASI), Via del Politecnico snc, 00133 Rome, Italy, Email: simone.pizzurro@asi.it*

agreement "Research and Development of a hypersonic demonstrator", which has the aim at completing the project Preliminary Design Review by 2025.

## 2. Scramjet configuration and mission description

The demonstrator design is based on the wave-rider concept, which aims to control shock waves generated during high-speed flight for producing lift and reducing drag.

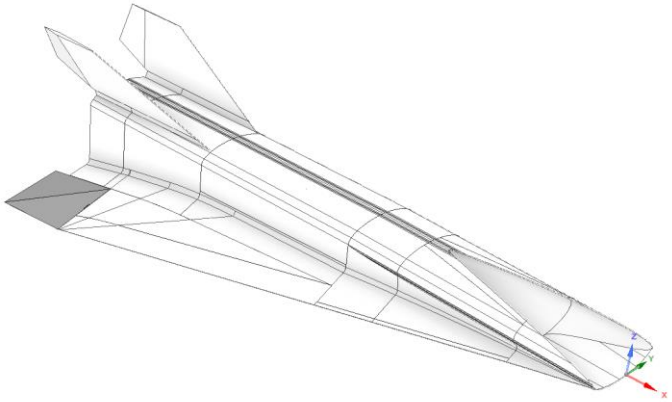

**Fig 1.** Demonstrator external configuration.

The SHEV demonstrator reference system as indicated in Fig 1 is body fixed, and its origin is located in the symmetry plane on the leading edge, where the X-axis pointed from leading to trailing edge, the Y-axis pointed towards the starboard wing and the Z-axis pointed upwards.
The hydrogen-fueled scramjet engine is strictly integrated into the demonstrator (see Fig 2) and is constituted just by open inlet, combustor and propulsive nozzle.

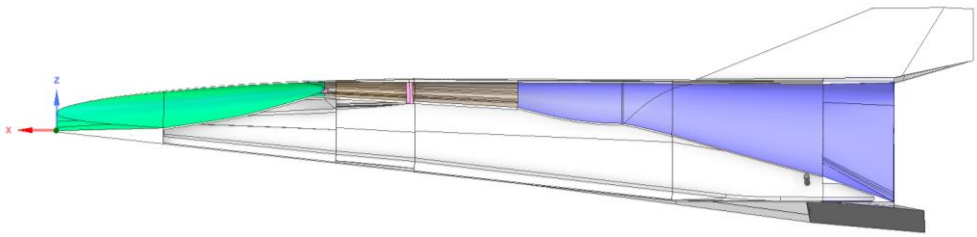

**Fig 2.** Internal path of demonstrator. Inlet (green), combustion chamber (brown), nozzle (violet), combustor's struts (pink).

The design emphasizes an elliptical intake with section contraction in the x-direction, following the Busemann model for minimal total pressure losses. The combustor has an elliptical section and is equipped with a two-stage multi-struts injector system, that is composed by two semi-struts, located at the beginning of combustor, and a full-strut located at the central zone of the same. The semi-struts distribute 65% of the hydrogen mass flow rate to the external regions; the central full-strut disperses the remaining quantity of fuel. The combustor is followed by the nozzle which transforms from elliptical section to almost circular one for improved expansion efficiency.

## 3. Mission description

The mission scenario is reported in Fig 3. It involves an air-launched solution with an aircraft carrier releasing (Sep 1) a launch system, consisting of the hypersonic demonstrator and its launch vehicle equipped by a booster, that brings the SHEV at specific speed and altitude. The launch system accelerates to the desired point and releases (Sep 2) the hypersonic demonstrator for a 10-second experimental operation. Computational Fluid Dynamics (CFD) analysis employed the free stream conditions chosen for experimental window (Mach 6÷8 and altitude 27÷32 km).

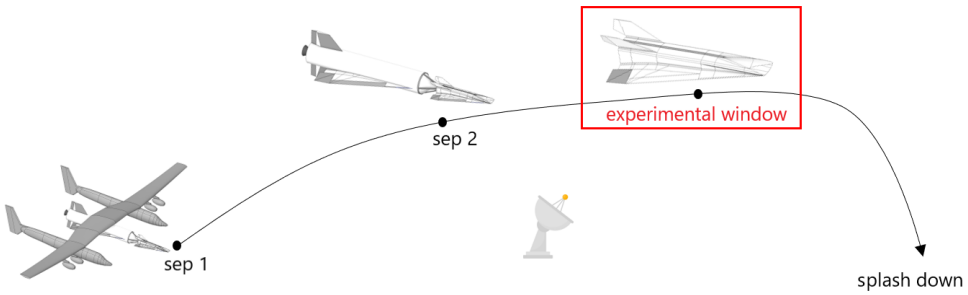


**Fig 3.** Mission scenario.

## 4. Numerical models and results

The performance evaluation of the scramjet engine was conducted by means of CFD analyses of the internal propulsive flow path. A simplified configuration was chosen focusing on half of the setup and employing an unstructured grid consisting of 1.9-million cells.
Proper grid blocks were added around the inlet and downstream of the propulsive nozzle to properly account for the interactions of internal flow with the external one.

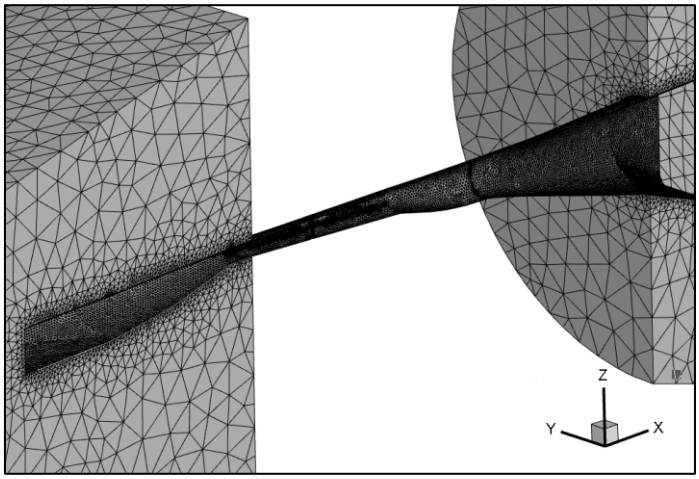


**Fig 4.** Computation grid for simulations.

### 4.1. Single-step reaction and viscous effect

In order to assess the air MFR (mass flow rate), under various conditions chosen for the experimental window, some preliminary numerical analyses were performed with inviscid flow and in fuel-off condition. Starting from the value of air MFR and maintaining a constant hydrogen-air equivalence ratio, ER, the mass flow rate of hydrogen can subsequently be computed by using the one step hydrogen-air chemical reaction (eq. 1).

$$2H_2 + O_2 + \frac{79}{21} N_2 \rightarrow 2H_2O + \frac{79}{21} N_2 \quad (1)$$

In the present paper, the stoichiometric air–fuel ratio for combustion has been assumed, which correspond ER equal to 1 and a ratio of hydrogen/air flow ratio equal to 0.02924.

$$ER = \frac{\left(\frac{\dot{m}_{fuel}}{\dot{m}_{air}}\right)}{\left(\frac{\dot{m}_{fuel}}{\dot{m}_{air}}\right)_{stoich}} = 1 \tag{2}$$

The waterfall scheme in Fig 5 recaps how the hydrogen mass fractions, that will be injected through the struts, were obtained according to the strategy previously exposed.

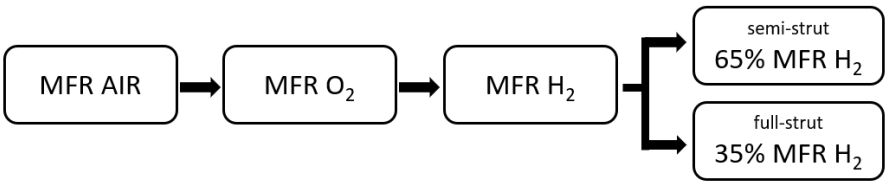


**Fig 5.** Waterfall scheme for computing $H_2$ mass fractions.

Further analyses have been performed to evaluate the effects of viscosity on internal propulsive flow path performance of SHEV. The Reynolds-Averaged Navier-Stokes (RANS) equations have been coupled with k–ω SST turbulence model. The quantities shown in the following figure represent the average values, integrated over different sections for some axial locations of the SHEV's propulsive flow path.

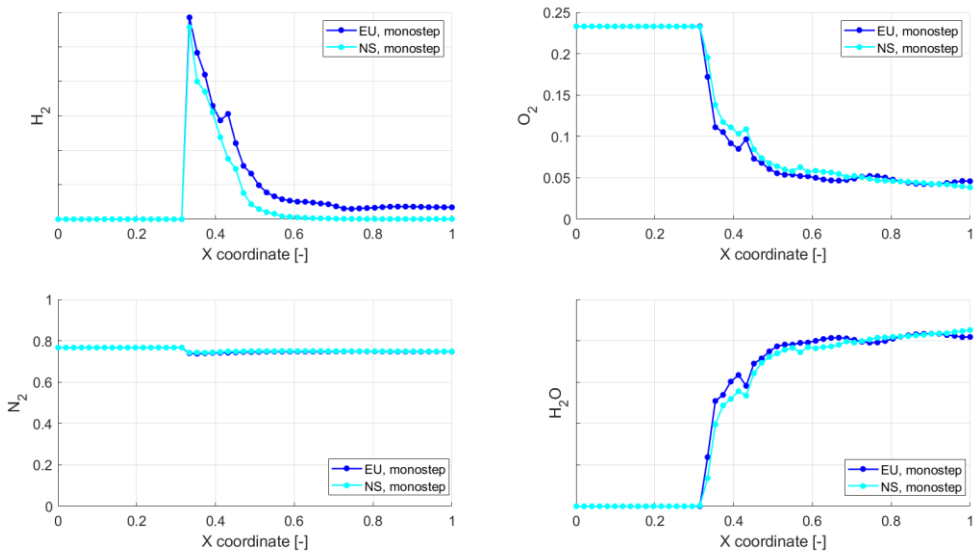


**Fig 6.** Comparison of averaged mass fractions profiles for different species along internal flow SHEV at the same altitude. Viscous (NS) and inviscid (EU) effect. Mono-step chemical model.

The distributions of the species involved in the single-step reaction are shown in Fig 6. The hydrogen mass fraction is zero up to the first injection, after there is a second weak peak associated to the second injection by full-strut. As evident from RANS results (NS) the peak appears to be dampened by the effect of viscosity. The mass fraction of nitrogen is almost unchanged, although a slight decrease in its mass fraction seems to be closely related to the hydrogen mass injection through the full-strut.

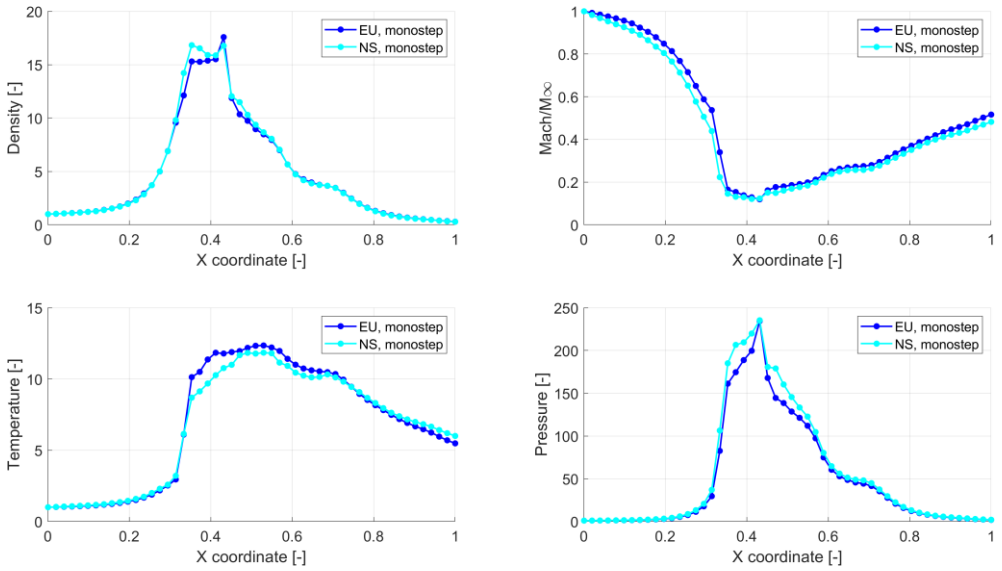


**Fig 7.** Comparison of thermodynamic and kinetic averaged parameters profiles along internal flow path of SHEV at the same altitude. Viscous (NS) and inviscid (EU) effect. Mono-step chemical model.

The thermodynamic and kinetic parameters in Fig 7 have been normalized with respect to free stream conditions. As can be seen in Fig 7, the addition of heat to the supersonic flow in the combustion chamber reduces the Mach number (in any case without causing thermal choking) and generates high pressure levels according to the Rayleigh flow theory. In the nozzle region, the Mach number increases first slightly and then significantly due to the substantial change in cross-section of the nozzle. This process converts thermal energy into kinetic energy as the flow expands, resulting in a decrease in temperature.

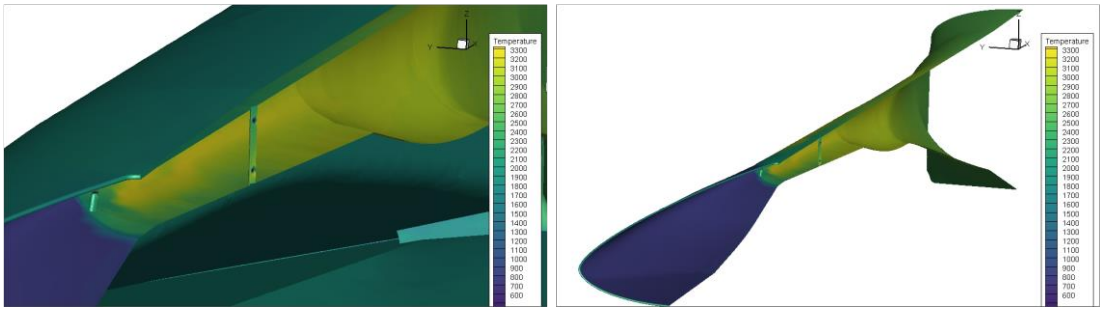

**Fig 8.** Temperature distributions on the inner walls of the propulsive duct.

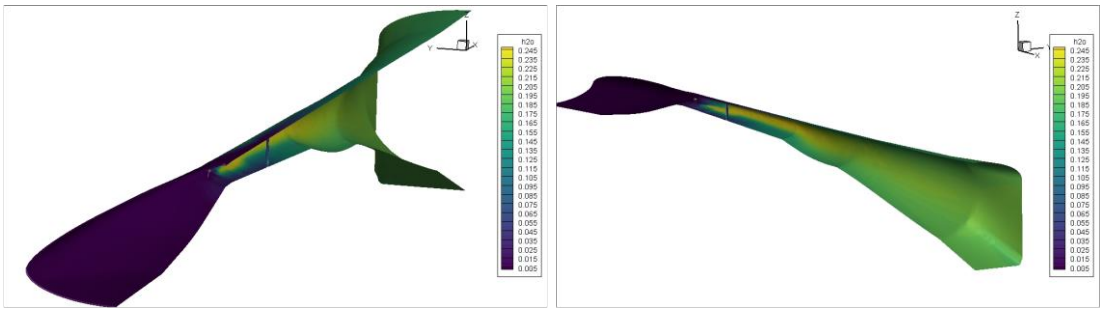

**Fig 9.** Distribution of water vapor inside the propulsion duct

In figures Fig 8 and Fig 9 are reported the temperature and water vapor surface distributions within the propulsive duct. It can be seen that the reaction takes place along the entire propulsive duct (combustion chamber and nozzle) leading to an increase in temperature. Due to the high temperature

value, the $H_2O$ species is in the gaseous state and, as also appears in Fig 6., is almost uniform in the nozzle region. One of the purposes of these simulations with single-step reaction is just to verify that combustion takes place satisfactorily.
The comparison between fuel-off and fuel-on conditions reported in Fig 10 shows the effect of the injection of hydrogen inside the combustion chamber. In particular, as depicted in figure, the effect on injection influences parameters such as the temperature, resulting in an approximate fivefold increase.

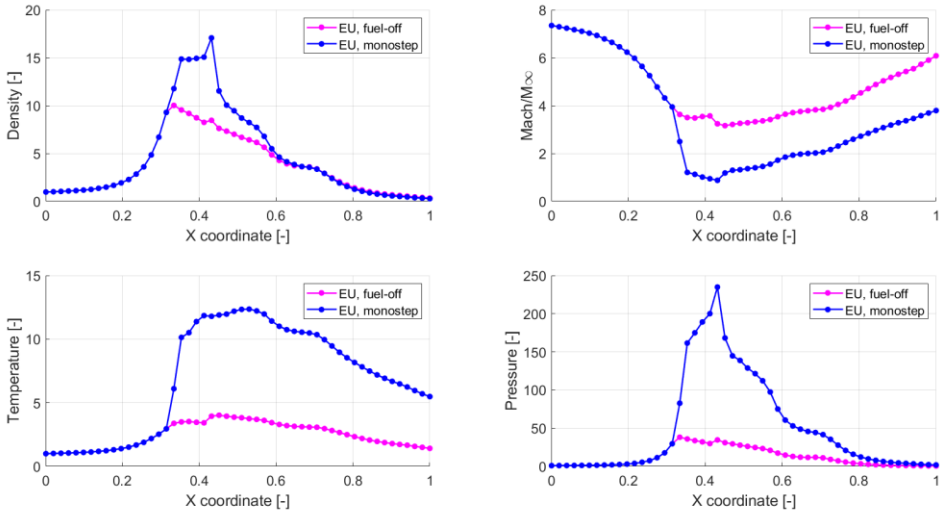


**Fig 10.** Comparison of thermodynamic and kinetic averaged parameters profiles along internal flow path of SHEV at the same altitude. Fuel-off and fuel-on conditions.

### 4.2. Multi-step reaction

In the context of the air-$H_2$ combustion mechanism, the reactants undergo a complex series of intermediate molecular transformations before giving the final products. The multistep reaction used in CFD simulations is the reduced Jachimowski chemical model for hydrogen-air combustion. The model includes 9 chemical species ($H_2$, $O_2$, $N_2$, $H_2O$, H, O, OH, N, and NO) and involves 12 reversible and elementary kinetic reactions [6] [7].

$$N_2 + O \leftrightarrow NO + N$$
$$O_2 + N \leftrightarrow NO + O$$
$$N + OH \leftrightarrow NO + H$$

**Table 1**: Zel'dovich mechanism for NO. [6] [7].

NO specie requires a careful consideration due to its particular role in emissions. The formation of nitric oxide is considered thanks to the Zel'dovich reactions (see Table 1) and is enhanced at elevated temperatures. This preference stems from the nitrogen molecule's triple covalent bond, imparting a drag to alter its molecular structure at lower temperatures; in fact, under such conditions, the nitrogen molecule exhibits non-reactive behavior and maintains a stable structure. At high temperatures the behavior of the $N_2$ molecule changes, making the molecule reactive and unstable. Notably, the heat generated (in this case during the combustion process) introduces agitation among the molecules, leading to the breaking of bonds within the nitrogen molecule. This phenomenon facilitates the initiation of reactions with oxygen that culminate in the formation of nitric oxide.
The comparison of section-averaged mass fractions of species involved in multi-step reactions at the two different altitudes considered is shown in Fig 11. Corresponding to the decrease in O and N species mass fractions, there is an increase in nitric oxide mass fraction.

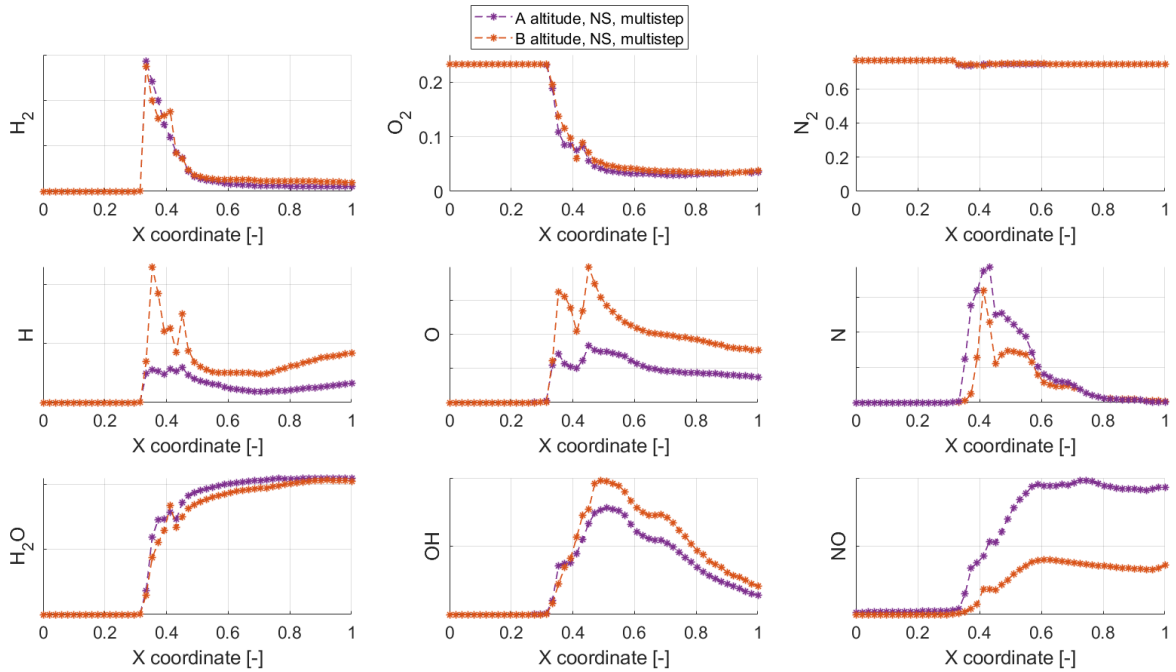


**Fig 11.** Comparison of averaged mass fractions profiles for different species along internal flow path of SHEV at two different altitudes. Viscous (NS) effect. Multi-step chemical model.

In particular, the distribution of NO (see also Fig 12) and $H_2O$ increase in the combustion chamber and remain nearly constant until the end of the engine duct, as well as the fuel ($H_2$) is almost completely burnt, see Fig 11.

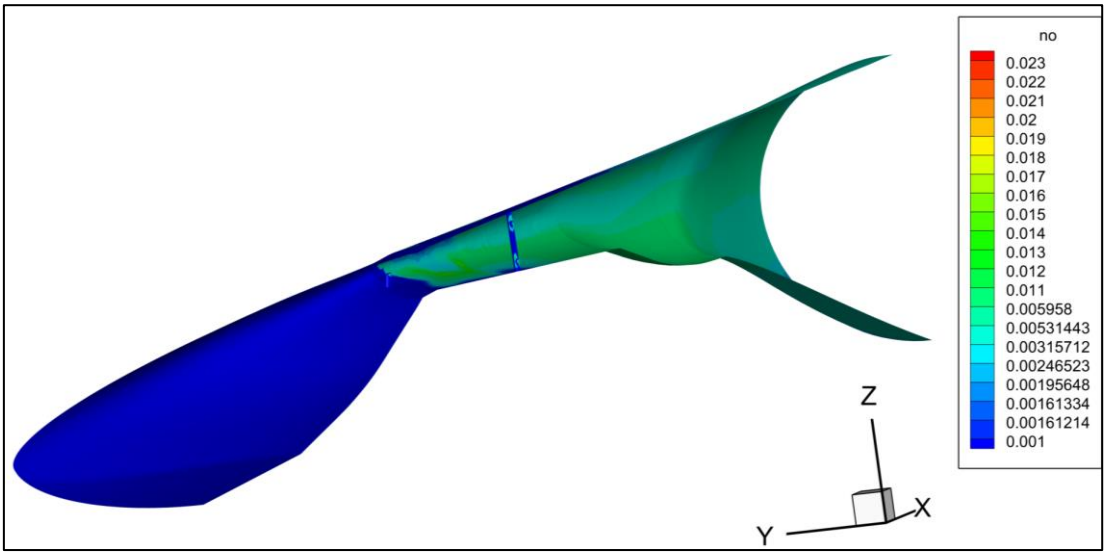


**Fig 12.** Distribution of NO species inside the propulsion flow path internal surface.

A full comparison of thermodynamic and kinetic averaged parameters at the same altitude are reported in Fig 13, showing also the effects of viscosity and air-hydrogen combustion modelling.

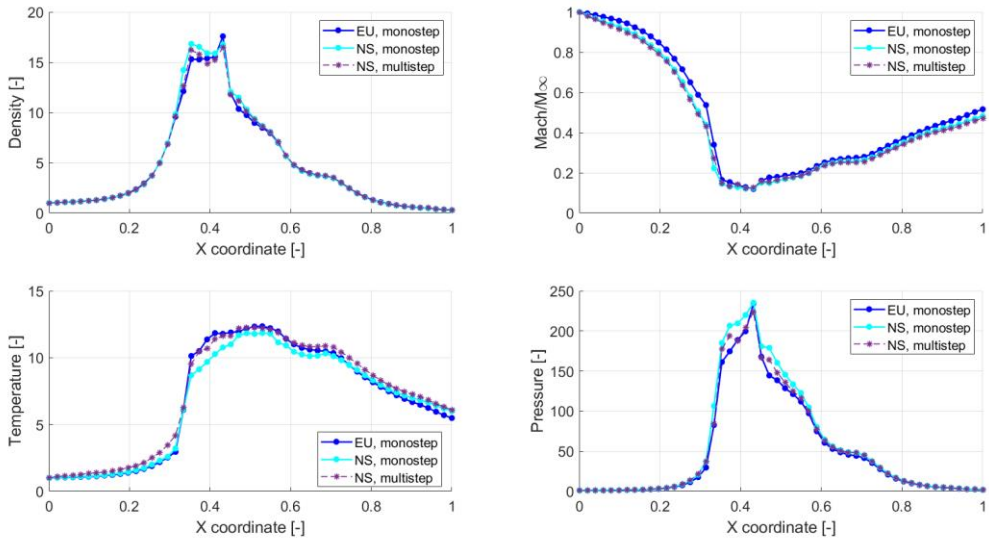


**Fig 13.** Comparison of thermodynamic and kinetic averaged parameters profiles along internal flow path of SHEV at the same altitude. Viscous (NS) and inviscid (EU) effect. Mono-step and multi-step chemical model.

### 4.3. Combustion efficiency

An important design parameter for the SHEV is combustion efficiency, $\eta_c$, defined as:

$$\eta_c = \frac{m_{H_2\ injected} - m_{H_2}}{m_{H_2\ injected}} = \frac{m_{H_2\ burned}}{m_{H_2\ injected}} \tag{3}$$

Combustion efficiency is a measure of how much of the fuel injected upstream has been burnt at that station. The following figure illustrates how the combustion efficiency, for the multi-step reactions modelling, is slightly lower than in the mono-step reaction modelling because, unlike the latter, in which the energy released by the chemical reaction is used exclusively for the formation of $H_2O$, in the multi-stage reactions a portion of the energy is also used for the formation of NO. In any case, the air-hydrogen combustion is basically completed in the combustor, where the combustion efficiency reaches a plateau due to frozen condition of the species.

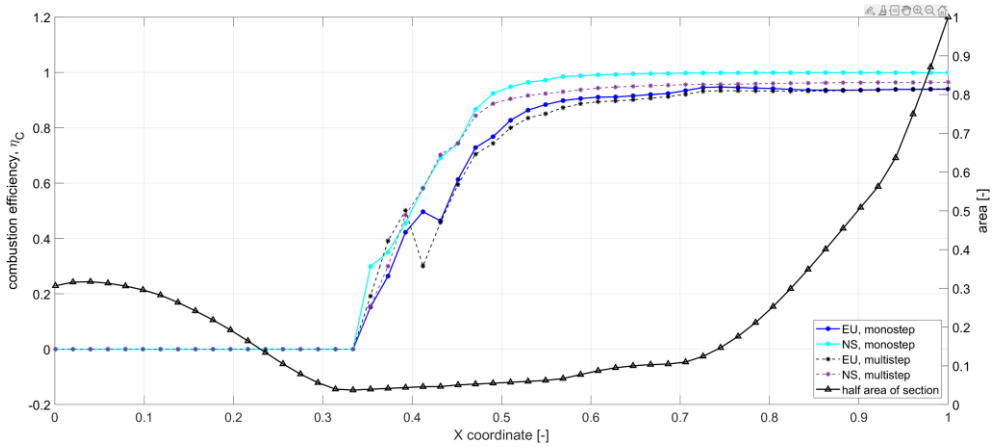


**Fig 14.** Comparison of combustion efficiency along internal flow path of SHEV. Viscous (NS) and inviscid (EU) effect. Multi-step chemical model.

## 5. Comparison between a full-scale configuration and a small-scale demonstrator

The CFD analyses of SHEV combustor's performance are compared with the results of the LAPCAT-II project full-scale hypersonic cruiser MR2.4 [8], these latter also supported by experimental test campaigns. In particular, the following figure shows the comparison of the combustion efficiency of the two combustors versus the axial coordinate normalized with respect to combustor's length. An important information obtained from the comparison concerns the efficiency value. In fact, the predicted values for the two combustors are very close to one despite being equipped with a different configuration of strut-injectors.

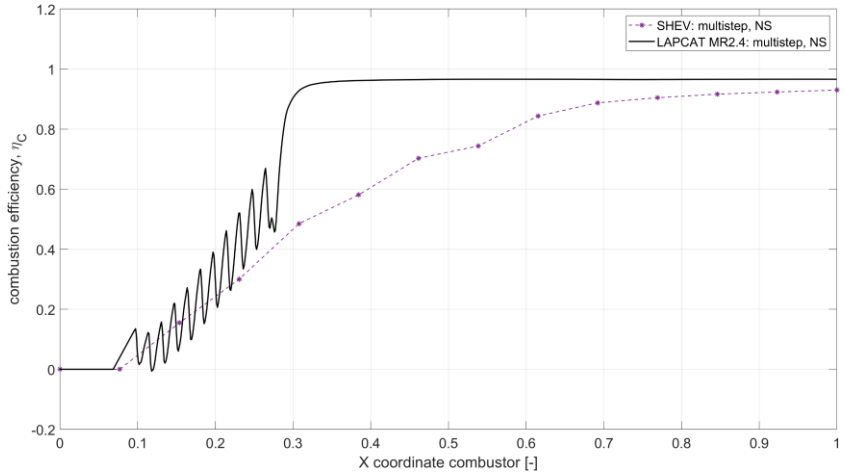


**Fig 15.** Comparison of combustion efficiency along combustor conduct. Viscous effect (NS). Multi-step chemical model. SHEV vs. LAPCAT-II MR2.4.

The scramjet combustor in the LAPCAT-II MR2.4 vehicle was equipped with a counter-V array of strut-injectors [8], as the oscillations of hydrogen mass-fraction clearly show in Fig 16., while, the injection of fuel in the SHEV combustor is impulsive and takes place in two different places (two symmetrical semi-struts at the beginning of combustor and a central full-strut located downstream). As shown in the same figure and confirmed by previous results, the viscous effects and consequent fuel mixing have dampened a lot the predicted values in terms of section-averaged distributions.

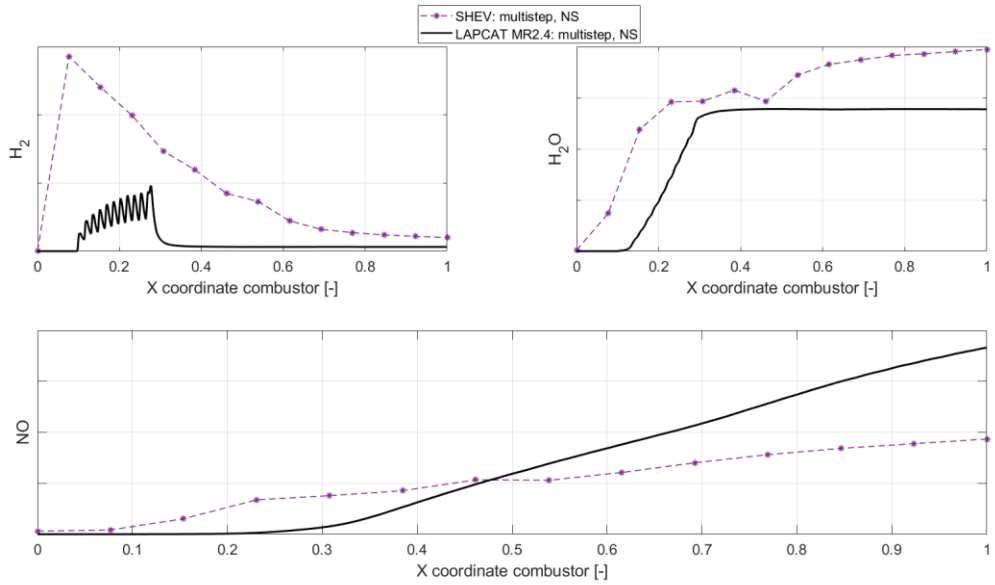


**Fig 16.** Comparison of averaged mass fractions profiles for different species along combustor conduct. Viscous effect (NS). Multi-step chemical model. SHEV vs. LAPCAT-II MR2.4.

## 6. Conclusions

The nose-to-tail CFD activities of the SHEV's scramjet propulsive flow path presented in this article have demonstrated that, in stoichiometric conditions, combustion take places completely in the combustor. The results obtained from the one-step reaction analysis for hydrogen-air combustion have provided a first understanding of the average trends of the thermodynamic and kinetic parameters in some points of the propulsive duct, characterized by multi-stage injection. The implementation in CFD simulations of Jachimowski's multi-step air-hydrogen combustion model has allowed a more detailed understanding of the behaviour of the species involved in the process, in particular in terms of nitric oxide thanks to the Zel'dovich reaction mechanism. The activation of viscosity model for CFD analysis with multi-step reactions, although very computationally expensive, is critical for a realistic prediction of the phenomenology and has indicated a combustion efficiency close to unity by the end of the combustor. This value is also confirmed by the comparison of results with the predicted data of MR2.4 full-scale hypersonic vehicle, deeply studied in the LAPCAT-II EC project.
Future actives will involve exploring the effect of the equivalence ratio on combustion performance, as in the case of lean and rich mixture fuel.

## Acknowledgements

The work has been co-funded by Italian Space Agency and CIRA ScPA in the frame of the agreement nr. 2022-13-HH.0-F43D22000410005.

## References

1. J. Steelant et al.: Conceptual Design of the High-Speed Propelled Experimental Flight Test Vehicle HEXAFLY". AIAA-2015-3539. 20th AIAA International Space Planes and Hypersonic Systems and Technologies Conference, Glasgow, Scotland, U.K. July 6-9, 2015.
2. Di Benedetto S., Di Donato M.P., Schettino A., Scigliano R., Nebula F., Morani G., Cristillo D., Marini M., Cardone S., Steelant J., Villace V.: The high-speed experimental flight test vehicle of HEXAFLY INT: a multidisciplinary design. CEAS Space Journal. (2021). DOI: 10.1007/s12567-020-00341-5.
3. Viola N., Fusaro R., Saracoglu B., Schram C., Grewe V., Martinez J., Marini M., Hernandez S., Lammers K., Vincent A., Hauglustaine D., Liebhardt B., Linke F., Fureby C.: Main Challenges and Goals of the H2020 STRATOFLY Project. Aerotecnica Missili & Spazio. (2021). 100:95–110, Published online: 29 May 2021, https://doi.org/10.1007/s42496-021-00082-6.
4. Viola N., Roncioni P., Gori O., Fusaro R.: Aerodynamic Characterization of Hypersonic Transportation Systems and Its Impact on Mission Analysis. MDPI-Energies. 16 June 2021. https://doi.org/10.3390/en14123580.
5. Mack A., Steelant J., Adirim H., Lentsch A., Marini M., Pilz N.: FAST20XX: Achievements on European Suborbital Space Flight. 7th European Symposium on Aerothermodynamics. Brugge. Belgium. May 2011.
6. Marini M., Saccone G., Chemical Kinetic Analysis of High-Pressure Hydrogen Ignition and Combustion toward Green Aviation. MDPI-aerospace. 25 January 2024.
7. Saccone G., Natale P., Marini M., Cutrone L., Hydrogen/Air Supersonic Combustion Modelling and Validation for Scramjet Applications, Journal of Fluid Flow, Heat and Mass Transfer (JFFHMT), doi: 10.11159/jffhmt.2022.017.
8. Roncioni P., Natale P., Marini M., Langener T., Steelant J., Numerical simulations and performance assessment of a scramjet powered cruise vehicle at Mach 8. Aerospace Science and Technology. Volume 42. 2015. ISSN 1270-9638.